# Bluer Phototruncation: Retro-Diels-Alder of Heptamethine Cyanine to Trimethine Cyanine through an Allene Hydroperoxide Intermediate

Lloyd Lapoot,<sup>1,2</sup> Connor Wang,<sup>3</sup> Siddharth S. Matikonda,<sup>3</sup> Martin J. Schnermann,<sup>3\*</sup> and Alexander Greer<sup>1,2,4\*</sup>

<sup>1</sup> Department of Chemistry, Brooklyn College, Brooklyn, New York, 11210, United States

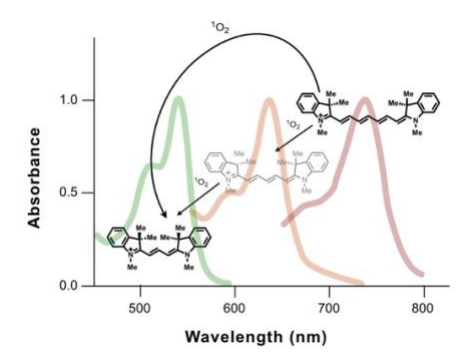
<sup>2</sup> Ph.D. Program in Biochemistry, The Graduate Center of the City University of New York, New York, 10016, United States

<sup>3</sup> Chemical Biology Laboratory, Center for Cancer Research, National Cancer Institute, Frederick, Maryland 21702, United States

<sup>4</sup> Ph.D. Program in Chemistry, The Graduate Center of the City University of New York, New York, New York, 10016, United States

 $Email\ addresses:\ martin.schnermann@nih.gov;\ agreer@brooklyn.cuny.edu$ 

# **Table of Contents Graphic**



# **Abstract**

The photoconversion of heptamethine to pentamethine cyanines and of pentamethine to trimethine cyanines was recently reported. Here, we report mechanistic studies and initial experimental evidence for a previously unexplored 4-carbon truncation reaction that converts the simplest heptamethine cyanine to the corresponding trimethine cyanine. We propose a DFT-supported model describing a singlet oxygen ( $^{1}O_{2}$ ) mediated formation of an allene hydroperoxide intermediate and subsequent 4-carbon loss through a retro-Diels-Alder process. Fluorescence and mass spectrometry measurements provide evidence for this direct conversion process. This 4-carbon truncation reaction adds to growing body of cyanine reactivity and may provide an optical tool leading to a substantial blue-shift ( $\Delta\lambda_{em}$ ) of ~200 nm.

# Introduction

Photoconversion reactions entail the conversion of one emissive species to another of different absorbance/emission wavelengths. In case of rhodamines and phenothiazines, such as

toluidine blue O, a photooxidative dealkylation reaction leading to substantial blue shift has been characterized in detail.<sup>1–3</sup> Another important class of probes are the cyanines, which have been used extensively as antibody and other biomolecule labels. Various studies had found that these molecules undergo photobluing processes, which was originally characterized as an artifact in various microscopy setting.<sup>4–13</sup>

Recent studies characterized the chemical basis of this photobluing process as the result of a photochemical 2-carbon loss, or phototruncation, reactions (Figure 1A). These reactions appear to involve the local photosensitized generation of singlet oxygen (<sup>1</sup>O<sub>2</sub>), which results in a reaction sequence that leads to the loss of 2 carbons from the polymethine chromophore. 14,15 These reactions were reported to occur between the various heptamethine cyanines, including the simplest, 1, and the corresponding pentamethine variant, 2. Additionally, 2, and other pentamethine cyanines that lack chromophore substitution were found to convert to the trimethine cyanine **3** by our groups and others. <sup>14–16</sup> Our prior study <sup>14</sup> proposed a <sup>1</sup>O<sub>2</sub>-based truncation reaction of the simplest heptamethine cyanine 1 to the corresponding pentamethine cyanine 2 through a multistep sequence. In this process, formation of peroxy intermediate arising from the attack of <sup>1</sup>O<sub>2</sub> on the C1' with subsequent hydration and elimination of a 2-carbon fragment (Figure 1B). The peroxy intermediate was hydrated at 1,2-position with formation of a hydroperoxyethanol intermediate with facile rotation about the C1'-C2' bond enabling an intramolecular formation of a hydroperoxycyclobutanol intermediate **D**. This chemistry has been applied for single molecule localization microscopy (SMLM) and cell-tracking strategies.

In the current work, we provide theoretical and experimental characterization for 4-carbon truncation for the direct conversion of heptamethine cyanine 1 to trimethine cyanine 3. In particular, our study provides mechanistic details on the theoretical chemistry of polyene 4, a

small-molecule model of **1**. We examine (1) whether the attack of  ${}^{1}\text{O}_{2}$  leads to peroxy and allene intermediates, (2) determine the role of conformation freedom, (3) explore the path to 4-carbon truncation, (4) investigate the process as concerted or stepwise; (5) and assess the experimental conversion of **1** to **3** upon 740 nm irradiation. The results obtained here point to a concerted 4-carbon loss process in **1** through 1,4-conjugate hydration and retro Diels-Alder truncation pathway (Figure 1C).

**Figure 1.** (A) Cyanine phototruncation. Irradiation of heptamethine **1** in PBS with 740 nm LED to reach pentamethine **2**, and irradiation of **2** with 630 nm LED to reach trimethine **3**. (B) Previous mechanistic proposal of cyanine phototruncation for conversion of **1** to **2** (as proposed in Ref. 14). (C) Proposed mechanism of cyanine truncation with the conversion of **1** to **3** by  ${}^{1}\text{O}_{2}$ . The mechanism features the formation of an allene hydroperoxide **E** and a retro-Diels-Alder reaction to reach **3**.

### **Result and Discussion**

Below we first describe the computational characterization of formation of a peroxy intermediate, allene hydroperoxide, and hydrolytic 4-carbon truncation process. A mechanistic analysis is then described, which is followed by supporting experimental results, and then our thoughts on broader implications of the study.

Theoretical Chemistry. Formation of Peroxy and Allene Hydroperoxide Intermediates. The calculated geometry of **4**, a small-molecule model of **1**, is shown in Figure 2. Figure 2 shows the first proposed step to be an asynchronous attack of  ${}^{1}O_{2}$  (an electrophilic species) on **4** at C1' leading to peroxy intermediate **5**. The results of natural bond orbital (NBO) calculations support this selectivity in **4** where the negative charges of -0.38 at C1' and -0.33 at C3' are more pronounced than that of -0.16 at C2' and of -0.12 at C4' (Table S1, Supporting Information). Addition of  ${}^{1}O_{2}$  to the C2' and C4' sites in **4** do not lead to minima, but only to  ${}^{1}O_{2}$ 's dissociation. An asynchronous attack of  ${}^{1}O_{2}$  on the C1' (**5a**) and C3' (**5b**) sites of **4** at C1' is 5.9 kcal/mol more stable than the peroxy intermediate at C3' (see Table S1, Supporting Information). For peroxy intermediate **5a**, the C1'–O1 bond length is 1.381 Å, and for peroxy intermediate **5b** the C3'–O1 bond length is 1.404 Å. The reaction of  ${}^{1}O_{2}$  on C1' of **4** is likely due to enhanced nucleophilicity, resulting in

peroxy intermediate 5a where NBO calculations show an attractive interaction of the outer oxygen atom (O2) with the C3'-H, where the C3'-H···O2 bond distance is 2.42 Å. This interaction is quantitated to be -1.4 kcal/mol. Next, we show a H-abstraction by O2 arises in an intramolecular reaction with a transition state barrier of 6.7 kcal/mol in an exothermic process to reach allene hydroperoxide 6. Notably, peroxy intermediates arise in other <sup>1</sup>O<sub>2</sub> oxidation reactions, such as R<sub>2</sub>S<sup>+</sup>OO<sup>-</sup> persulfoxide, and have been implicated in lowering of rotational energy barriers. <sup>17-19</sup> Similarly, allene hydroperoxides and hydroxides have been previously reported in <sup>1</sup>O<sub>2</sub> oxidation of diene and trienes, and are structurally reminiscent of allene hydroxides.<sup>20–27</sup> The protonation and hydration reactions suggest a zwitterionic form of the peroxy intermediate rather than a diradical formation. We note that Li and Smith<sup>28</sup> have reported that long-term storage of indocyanine green under low-intensity light leads to oxidative dimer formation likely via radical intermediates formed by electron transfer to form superoxide, dimerization, and subsequent hydrogen-atom abstraction reaction. For 6, NBO results show a H-bond of the O2-H with the allene C3'=C4' π bond quantitated to be -1.8 kcal/mol. Protonation and hydroxylation of allene hydroperoxide 6 are proposed as key next steps.

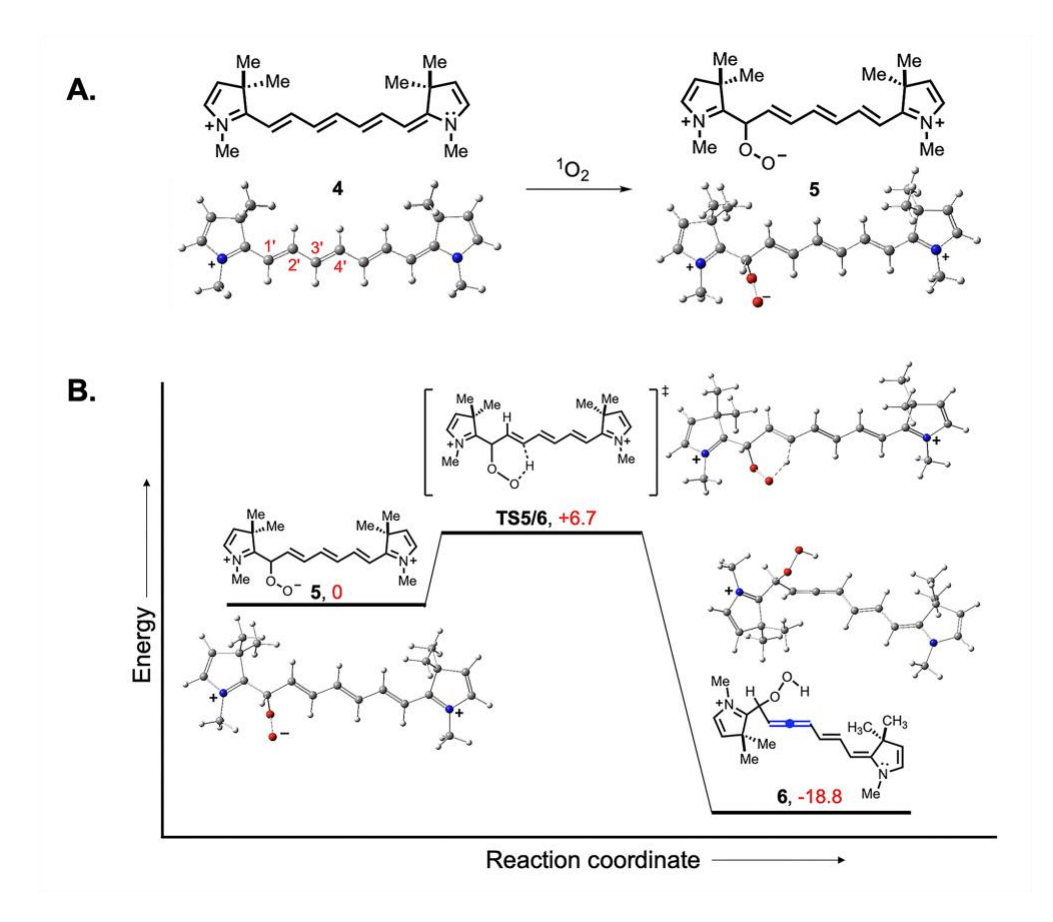


**Figure 2.** (a) Calculated addition of  ${}^{1}O_{2}$  to the C1' of **4** to reach peroxy intermediate **5**. (b) Computed potential energy surface for the conversion of **5** to **6** using M062-X/6-31+G(d,p). Relative enthalpies ( $\Delta H$ ) are given in kcal/mol.

*Protonation and Hydration*. Next, we explored the protonation of allene hydroperoxide **6** at C2', C3', and C4' (Figure 3). From **6**, two routes lead to a *cis*-configuration: the first is bottom-face protonation of C3' giving **8** in the *s-cis* conformation, and the second is via protonation at C4'

with proton migration to C3' giving **9** in the *s-trans* conformation. The transition state barrier between *s-trans* **9** and *s-cis* **8** is 8.6 kcal/mol and endothermic by 7.2 kcal/mol is mainly attributed to increased congestion in the *s-cis* form. The top-face protonation at C3' could reach *trans* **7**, but is blocked by a π H-bond between O2–H and allene C3'=C4', despite being the most stable in the series, **7-9**. Protonation at C2' could conceivably lead to **10**, but is energetically prohibited. Next, we focused on the hydroxylation step. Hydroxylation at C4' of **8** in the *s-cis* conformation results to the formation of C1'-peroxy, C4'-hydroxy intermediates *cis-syn* **11** and *cis-anti* **12** with the former more stable by 5.5 kcal/mol (Figure 4). Alternatively, hydroxylation at C4' of **9** in the *s-trans* conformation also results in formation of *cis-syn* **11** and *cis-anti* **12**. Upon forming the 1,4-hydroperoxybutanols **11** and **12**, a *cis* configuration exists about the C2'=C3' double bond setting up an intramolecular attack in formation of a 6-membered ring and subsequent 4-carbon fragmentation in a retro-Diels-Alder reaction, as we have been alluding to.

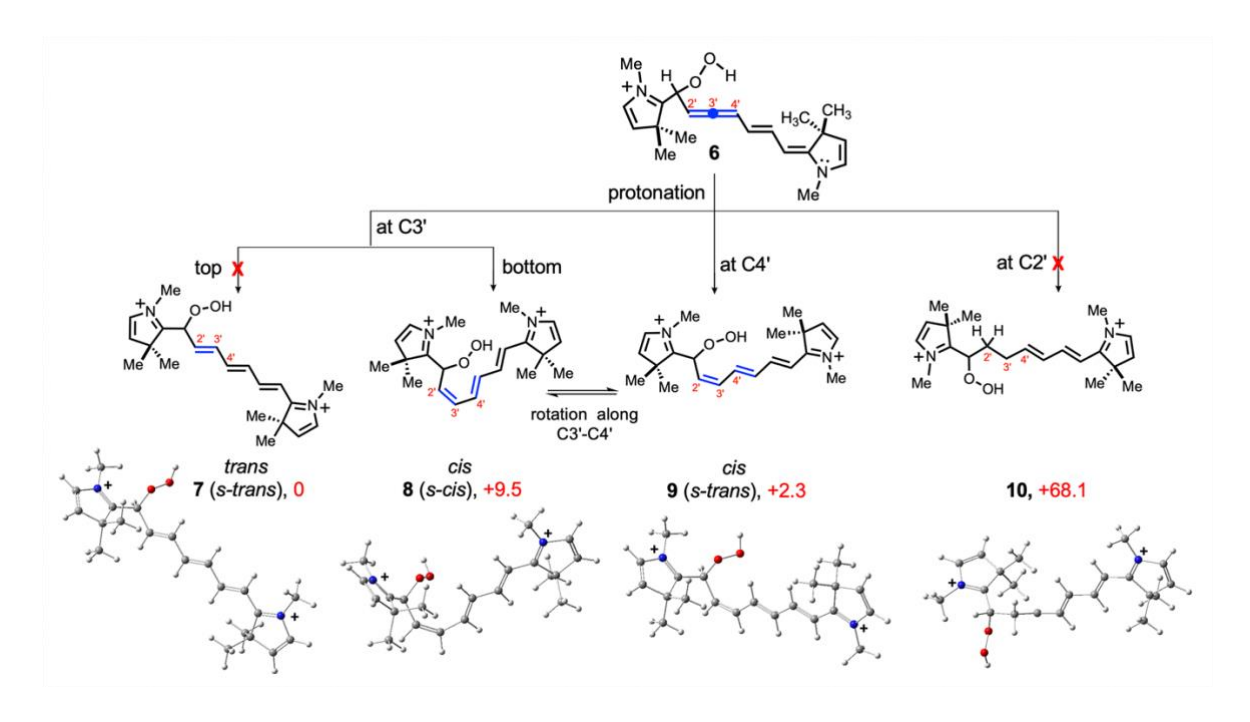


**Figure 3**. DFT-computed energies for the protonation of **6**. Relative enthalpies ( $\Delta H$ ) are given in kcal/mol.

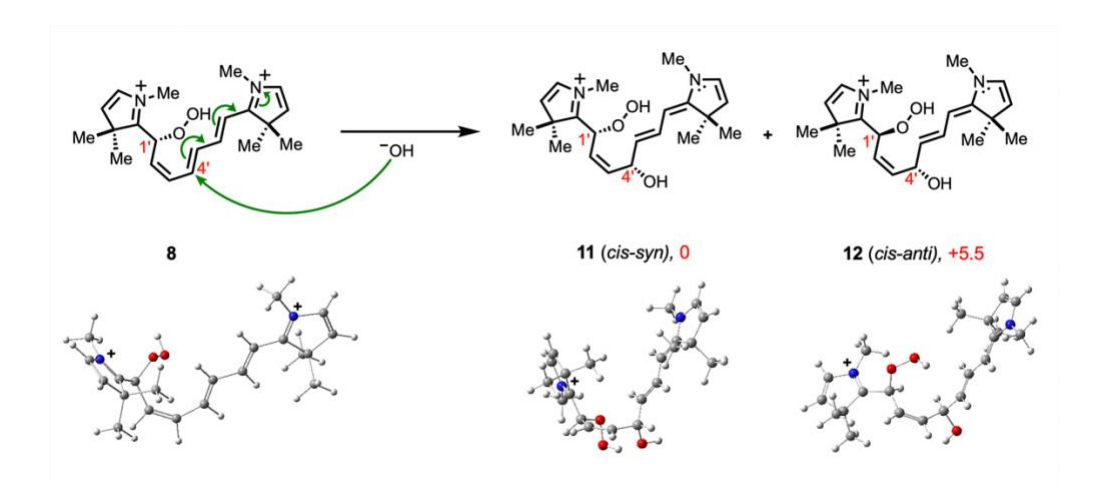


**Figure 4.** DFT-computed energies for the addition of hydroxide ion to **8**. Relative enthalpies ( $\Delta H$ ) are given in kcal/mol.

Formation of a 6-membered ring and subsequent retro-Diels-Alder reaction (Figure 5). On forming the 1,4-hydroperoxybutanols 11 and 12, this paves the way for a facile rotation along the C1'-C2' and C3'-C4' single bonds, respectively. The results show that conformer 13 brings C1 and C5' into close proximity for an intramolecular formation of 6-membered ring intermediate 14 with an activation energy of 3.3 kcal/mol and exothermic by 10.4 kcal/mol. A retro-Diels-Alder reaction ensues with conversion of 14 to concerted loss of a 4-carbon fragment hydroperoxybutenol (HOOCH=CHCH=CHOH) 15 and truncated 16 through transition state TS14/15-16 (50.7 kcal/mol) in a process exothermic by 1.3 kcal/mol. Mapping out the potential energy surface with desmethyl 13 (gem-dimethyls removed) produced some differences with a transition state energy of 43.6 kcal/mol reflect the effect of congestion due to the bulky methyl substituents, in which the reaction is exothermic by 1.7 kcal/mol. In Figure 5, values for the relative Gibbs free energies (in green) shows minor differences when compared to the relative enthalpies. For example, the Gibbs free energy for the formation of the six-membered ring intermediate 14 via TS13/14 is exergonic by 9.4 kcal/mol, and the conversion of 14 to 15 and truncated 16 via TS14/15-16 is exergonic by 3.3 kcal/mol. We surmise that the energies are dependent on conformational aspects for the 6-membered ring formation and subsequent 4-carbon fragmentation calculated. We suggest that the relatively high computed transition state barriers (43.6-50.7 kcal/mol) is compensated by the loss of the 4-carbon fragment 15 in a entropy-driven process and favorable in terms of free energy, in which barrier reductions could follow with inclusion of implicit and explicit solvent effects. However, we note that computed activation energies for experimentally observed retro-Diels-Alder reactions have been reported, and also tend to be high, <sup>29</sup>

in which solvent polarity and electron donating and sometimes electron withdrawing substituents can lower it.<sup>30</sup> Interestingly, activation energies reported for retro-Diels-Alder reactions span a range of ~30 to 145 kcal/mol. A stepwise retro-Diels-Alder process was not found in our system, although it has been reported in other systems, such as partially saturated 2-pyrones.<sup>31,32</sup> Next, experimental studies were carried out to examine whether a 4-carbon phototruncation process occurs in heptamethine cyanine and also whether buffer conditions can increase this process.

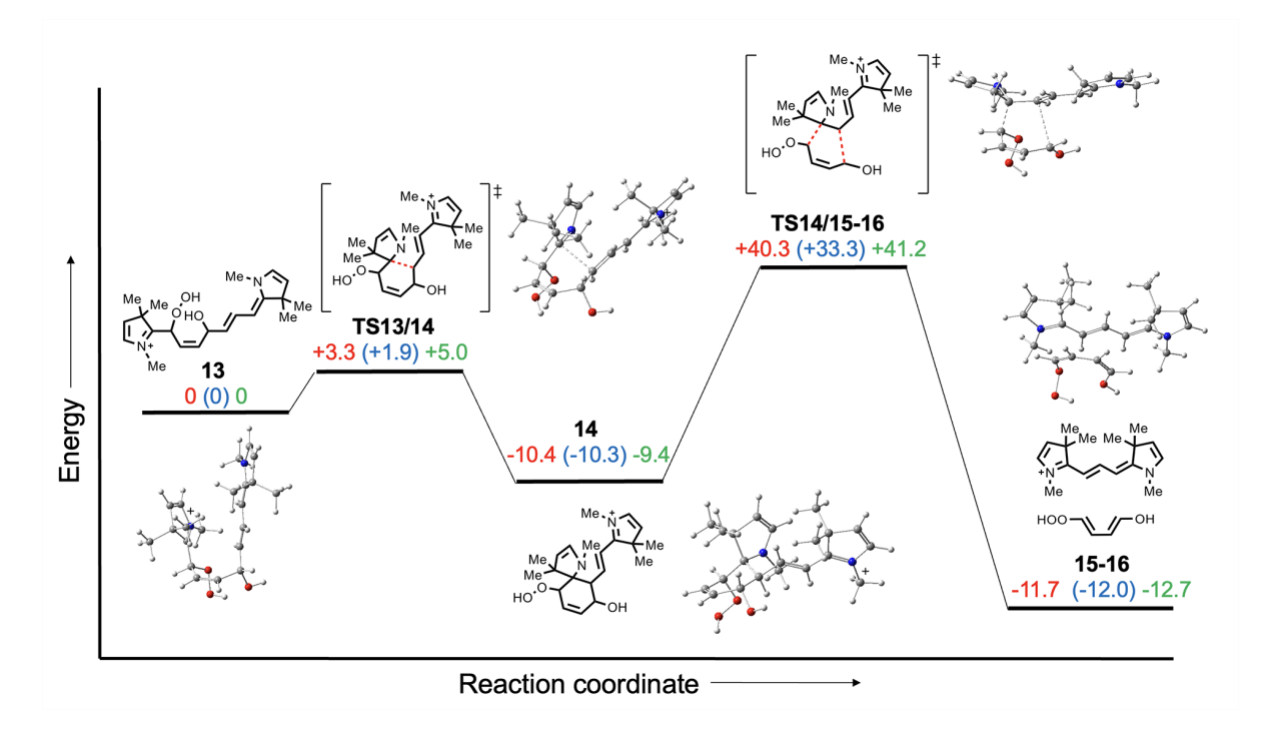
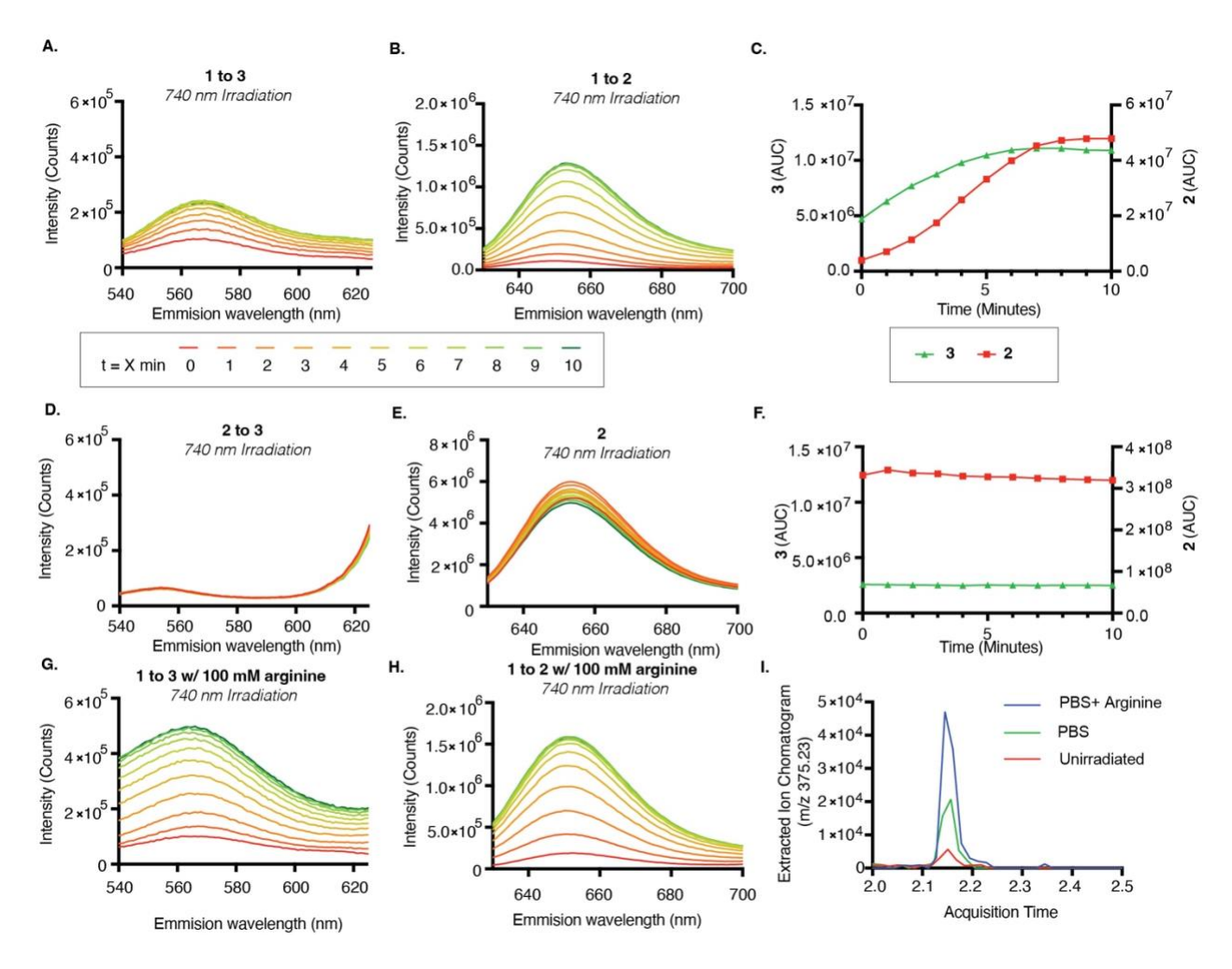


Figure 5. DFT-computed energies for the interconversion of conformer 13. Relative energies in red are for the conversion of 13 to 15; relative energies in blue are for structures absent of *gem*-dimethyl groups. Relative enthalpies ( $\Delta H$ ) are in red and blue and relative free energies ( $\Delta G$ ) are in green (kcal/mol).

**Experimental Chemistry.** In prior studies examining the conversion of 1 to 2, we initially noted the formation of further blue shifted products. Here we set out to characterize these products in greater detail. Specifically, we found that monitoring the 740 nm LED irradiation using fluorescence based measurement with a 25 µM solution of 1 in pH 9 PBS lead to the formation of both the previously observed 2, but also a new peak with identical emission properties to 3, albeit to a lesser degree (Figure 6A-C). We then sought to assess if the formation 3 occurred by the conversion of 1 initially to 2 and then onward to 3. To test this, a 2.5 µM solution of 2 in pH 9 PBS was irradiated under identical conditions (Figure 6D-F). No meaningful formation of 3 was observed. In our prior work, we found that a number of additives improved the conversion of 1 to 2.14 After testing, we found that the addition of arginine (100 mM in pH 9 PBS) enhanced that conversion of the reaction, by about ~2 fold (Figure 6G and H). Finally, the identity of 3 and the observation that arginine enhance the conversion was also confirmed by HRMS studies (Figure 6I). The initial experimental studies presented here provide key evidence suggesting that 1 converts directly to 3 via a retro-Diels-Alder reaction. Future efforts to define the role of conversion of this are likely merited.



**Figure 6.** Photoconversion of **1** in pH 9.0 PBS with 740 nm irradiation. (a) Fluorescence signal (510 nm excitation) over 10 minutes. (b) Fluorescence signal (620 nm excitation) over 10 minutes. (c) Integrated fluorescence signal **for 2** and **3** from (a) and (b) over the course of 10 minutes. Control reaction of **2** in pH 9.0 PBS with 740 nm irradiation. (d) Fluorescence signal (510 nm excitation) over 10 minutes. (e) Fluorescence signal (620 nm excitation) over 10 minutes. (f) Integrated fluorescence for **2** and **3** from (d) and (e) over the course of 10 minutes. Photoconversion from **1** in pH 9 PBS w/ 100 mM Arginine with 740 nm irradiation. (g) Fluorescence signal (510 nm excitation) over 10 minutes. (h) Fluorescence signal (620 nm excitation) over 10 minutes. (i)

Extracted ion chromatogram (EIC) for 3 (m/z = 357.23) in control (PBS, unirradiated), PBS (740 nm irradiation), and PBS with 100 mM arginine (740 nm irradiation) conditions.

### Conclusion

These studies indicate that heptamethine cyanines undergo a photochemical 4-carbon loss reaction in certain settings. These efforts add to the rich photochemistry of cyanines, reactions with implications in a range of microscopy and imaging settings. 12,33 Our computational and experimental results suggest a multistep pathway leading to 4-carbon excision. Specifically, the following conclusions were drawn from the DFT results (1) a peroxy intermediate is formed in the initial reaction of cyanine with  ${}^{1}\text{O}_{2}$ , which undergoes abstraction of C3'–H to reach an allene hydroperoxide, (2) allene hydroperoxide protonation and 1,4-hydroxylation hydrolysis lead to a C1'–peroxy-C4'-hydroxy intermediate, (3) conformational freedom and *cis*-geometry along the C2'–C3' bond allow for the formation of the 6-membered ring intermediate to be in close proximity for an intramolecular attack. (4) A 4-carbon truncation of hydroperoxybutenol (HOOCH=CHCH=CHOH) ensues, by a proposed concerted retro-Diels-Alder process. Our experimental data to date provides key evidence that this chemistry occurs in direct fashion and that the reaction can be enhanced by the addition of an arginine additive. Further studies to characterize the role of the additive and to possibly exploit this chemistry are underway.

# Methods

Computational Methods. DFT calculations were conducted with Gaussian 16,  $^{34}$  in which optimizations were carried out with M062X $^{35}$  and the basis set 6-31+G(d,p) $^{36-38}$  in the gas phase,

which reportedly perform well.<sup>39,40</sup> Energies were calculated based from the zero-point energy (ZPE) calculations at 298 K and ΔG energies were computed in Figure 5.<sup>41</sup> Solvent effects were not calculated. Frequency calculations and intrinsic reaction coordinate (IRC) calculations were conducted to substantiate transition structures and their connectivity to reagents and products. Molecular orbital interactions were studied with determined natural bonding orbital (NBO) calculations using NBO 7.0.<sup>42</sup> Spin contamination was examined for M06-2X/6-31+G(d,p) optimized structure **J** using T1 diagnostics using DLPNO-CCSD(T)/aug-cc-pVTZ and found to be 0.015.<sup>43–46</sup> These results indicate an acceptable level of spin contamination that is not a significant issue for the reaction system, where T1 values that are greater than 0.02 for closed-shell systems or greater than 0.03 for open-shell systems point to unacceptable non-dynamical correlation or multiconfigurational character effects.

Experimental Methods. All commercially obtained reagents were used as received. Cyanines 1 and 2 were acquired from Sigma-Aldrich and purified by reversed phase chromatography. The crude mixture was dissolved in 5% MeCN:H<sub>2</sub>O and purified over reverse phase chromatography (5-50% MeCN:H<sub>2</sub>O) to provide the desired product. Data analysis and curve fitting were performed using MS Excel 2011 and GraphPad Prism 7. Light intensity measurements were performed with a Thorlabs PM200 optical power and energy meter fitted with an S120VC standard Si photodiode power sensor (200-1100 nm, 50 nW to 50 mW).

Irradiation samples were prepared using a DMSO parent stock (2.2 mM for heptamethine cyanine and 2.5 mM for pentamethine cyanine) that was then serially diluted to a final

concentration of 20 µM in the respective buffer (PBS pH 9 or PBS pH 9 with 100 mM L-arginine). These samples were placed into 3.5 mL quartz cuvettes and left for 30-60 minutes in the dark to equilibrate. The cuvettes were then placed into a 3D-printed irradiation apparatus with a Mightex 740 nm standard range LED with cooling fan that was powered by a Mightex LED driver with manual and analog input control (SLA series) as well as an Edmund Optics 720 nm long-pass filter. With the LED driver set to maximum power (1000 mA) a light intensity of approximately 1 W cm<sup>-2</sup> was achieved throughout the 10-minute irradiation at 22 °C. The initial, intermediate, and final fluorescence measurements were made using a Horiba PTI QuantaMaster 8075-11-C spectrophotometer. Controlled via FelixGX software, two measurement presets were used: one intended to capture the presence of 3 with irradiation at 510 nm, 5 nm excitation slit widths and 10 nm emission slit widths (for both entrance and exit slits), emission measurement from 530 nm to 700 nm, and a step size of 1 nm with an integration time of 0.1 s; likewise, a second preset was used to capture the presence of 1 and 2 with irradiation at 620 nm, 5 nm excitation and emission slit widths (for both entrance and exit slits), emission measurement from 630 to 850 nm, and a step size of 1 nm with an integration time of 0.1 s.

Samples used for mass spectrometry were prepared in a similar manner, only with a higher concentration (100  $\mu$ M) and a longer irradiation time (25 min). After the completion of the irradiation, the samples were mixed with 4-6 mL of DCM to extract the fluorophore mixture. The DCM solution was then dried through a sodium sulfate column. The eluted solutions were then dried via nitrogen gas and resuspended in 100  $\mu$ L acetonitrile and placed into HPLC vials. Mass spectrometry data was acquired on an Agilent 6520 Accurate-Mass Q-TOF LC/MS System, (Agilent Technologies, Inc., Santa Clara, CA) equipped with a dual electro-spray source, operated in the positive-ion mode. Separation was performed on Zorbax 300SB-C18 Poroshell column (2.1

mm x 150 mm; particle size 5 μm). The analytes were eluted at a flow rate of 1 ml/min with a 5 to 100% organic gradient over 4 minutes and holding organic for 1 minute, where 0.1% aqueous formic acid was exchanged for 0.1% formic acid in acetonitrile. The instrument was used in either full-scan TOF mode. MS source parameters were set with a capillary voltage of 4 kV, the fragmentor voltage of 150 V and skimmer 65 V. The gas temperature was 350 °C, drying gas flow 12 L/min and nebulizer pressure 55 psig. Data were acquired at high resolution (1,700 m/z), 4 GHz. To maintain mass accuracy during the run time, an internal mass calibration sample was infused continuously during the LC/MS runs. Data acquisition and analysis were performed using MassHunter Workstation Data Softwares, LCMS Data Acquisition (version B.06.01) and Qualitative Analysis (version B.07.00).

### **ASSOCIATED CONTENT:**

# • Data Availability Statement

The data underlying this study are available in the published article and its Supporting Information.

# • Supporting Information Statement

Supporting Information is available, including information about the computer cluster used, descriptions of energies and geometries of stationary points, a table of computed parameters for **4**, **5a**, and **5b**, and mass total ion and extracted ion count data in Figure 6I.

# **ORCID**

Lloyd Lapoot: 0000-0001-6888-2626

Connor Wang: 0009-0005-8389-7793

Martin J. Schnermann 0000-0002-0503-0116

Siddharth S. Matikonda 0000-0002-3875-5762

Alexander Greer: 0000-0003-4444-9099

Acknowledgments

L.L. and A.G. thank the National Science Foundation (CHE-2154133) for funding. S.S.M. and

M.J.S. were supported by the Intramural Research Program of the National Institutes of Health,

National Cancer Institute (NCI), Center for Cancer Research. This work used Expanse in the

Extreme Science and Engineering Discovery Environment (XSEDE) cluster at the San Diego

Supercomputer Center, which is supported by the NSF (ACI-1548562) through allocation CHE-

210052. We also thank Leda Lee for the graphic arts work and the Biophysics Resource in the

Structural Biophysics Laboratory, Center for Cancer Research, NCI at Frederick for assistance

with liquid chromatography-mass spectrometry analysis.

References

1. Robinson-Duggon, J.; Marino-Ocampo, N.; Barrias, P.; Zuniga-Nunez, D.; Gunther, G.;

Edwards, A. M.; Greer, A.; Fuentealba, D. Mechanism of Visible-Light Photooxidative

Demethylation of Toluidine Blue O. J. Phys. Chem. A. 2019, 123, 4863–4872.

2. Butkevich, A. N.; Bossi, M. L.; Lukinavicius, G. v.; Hell, S. W. Triarylmethane Fluorophores

Resistant to Oxidative Photobluing. J. Am. Chem. Soc. 2019, 141, 981–989.

- 3. Evans, N. Photofading of Rhodamine Dyes: Identification of Some Rhodamine B Photoproducts. *J. Soc. Dyers Colour* **1970**, *86*, 174–177.
- 4. Tatikolov, A. S. Polymethine Dyes as Spectral-Fluorescent Probes for Biomacromolecules. *J. Photochem. Photobiol. C* **2012**, *13*, 55–90.
- 5. Lin, C.-M.; Usama, S.; Burgess, K. Site-Specific Labeling of Proteins with Near-IR Heptamethine Cyanine Dyes. *Molecules* **2018**, *23*, 2900.
- Sapozhnikova, K. A.; Misyurin, A. V.; Pestov, N. B.; Meleshkina, E. G.; Oreshkov, S. D.; Ganzhula, E. P.; Mikhailova, A. S.; Korshun, V. A.; Misyurin, V. A.; Brylev, V. A. Detection of the PRAME Protein on the Surface of Melanoma Cells Using a Fluorescently Labeled Monoclonal Antibody. *Russ. J. Bioorg. Chem.* 2021, 47, 1077–1085.
- Ingenhoven, N.; Beck-Sickinger, A. G. Fluorescent Labelled Analogues of Neuropeptide Y for the Characterization of Cells Expressing NPY Receptor Subtypes. *J. Recep. Sig. Trans.* 1997, 17, 407–418.
- 8. Nguyen, B.; Ciuba, M. A.; Kozlov, A. G.; Levitus, M.; Lohman, T. M. Protein Environment and DNA Orientation Affect Protein-Induced Cy3 Fluorescence Enhancement. *Biophys. J.* **2019**, *117*, 66–73.
- 9. Cheng, C.; Trzcinski, O.; Doering, L. C. Fluorescent Labeling of Dendritic Spines in Cell Cultures with the Carbocyanine Dye. *Front. Neuroanat.* **2014**, *8*, 1-8.
- 10. Flors, C. Photoswitching of Monomeric and Dimeric DNA-intercalating Cyanine Dyes for Super-Resolution Microscopy Applications. *Photochem. Photobiol. Sci.* **2010**, *9*, 643–648.
- 11. Chen, S.; Wang, J.; Xin, B.; Yang, Y.; Ma, Y.; Zhou, Y.; Yuan, L.; Huang, Z.; Yuan, Q. Direct Observation of Nanoparticles within Cells at Subcellular Levels by Super-Resolution Fluorescence Imaging. *Anal. Chem.* 2019, 91, 5747–5752.
- 12. Gorka, A. P.; Nani, R. R.; Schnermann, M. J. Harnessing Cyanine Reactivity for Optical Imaging and Drug Delivery. *Acc. Chem. Res.* **2018**, *51*, 3226–3235.

- 13. Sun, C.; Du, W.; Wang, B.; Dong, B.; Wang, B. Research Progress of Near-Infrared Fluorescence Probes Based on Indole Heptamethine Cyanine Dyes *in vivo* and *in vitro*. *BMC Chem.* **2020**, *14*, 21.
- 14. Matikonda, S. S.; Helmerich, D. A.; Meub, M.; Beliu, G.; Kollmannsberger, P.; Greer, A.; Sauer, M.; Schnermann, M. J. Defining the Basis of Cyanine Phototruncation Enables a New Approach to Single-Molecule Localization Microscopy. ACS Cent. Sci. 2021, 7, 1144–1155.
- 15. Helmerich, D. A.; Beliu, G.; Matikonda, S. S.; Schnermann, M. J.; Sauer, M. Photoblueing of Organic Dyes can Cause Artifacts in Super-Resolution Microscopy. *Nat. Methods* **2021**, *18*, 253–267.
- 16. Cho, Y.; An, H. A.; Kim, T.; Lee, C.; Lee, N. K. Mechanism of Cyanine5 to Cyanine3 Photoconversion and Its Application for High-Density Single-Particle Tracking in a Living Cell. *J. Am. Chem. Soc.* **2021**, *143*, 14125–14135.
- 17. O'Shea, K. E.; Foote, C. S. Chemistry of Singlet Oxygen. 51. Zwitterionic Intermediates from 2,4-Hexadienes. *J. Am. Chem. Soc.* **1988**, *110*, 7167–7170.
- 18. Turque, O.; Greer, A.; Wauchope, O. R. Synthetic Feasibility of Oxygen-Driven Photoisomerizations of Alkenes and Polyenes. *Org Biomol Chem* **2020**, *18*, 9181–9190
- 19. Turque, O.; O'Connor, R. M.; Greer, A. Singlet Oxygen's Potential Role as a Nonoxidative Facilitator of Disulfide S–S Bond Rotation. *Photochem. Photobiol.* **2023**, *99*, 652-660.
- 20. Foote, C. S.; Brenner, M. Chemistry of Singlet Oxygen. *Tetrahedron Lett.* **1968**, *9*, 6041–6044.
- 21. Stratakis, M.; Orfanopoulos, M. Regioselectivity in the Ene Reaction of Singlet Oxygen with Alkenes. *Tetrahedron*, **2000**, *56*, 1595–1615.
- 22. Mori, H.; Ikoma, K.; Masui, Y.; Isoe, S.; Kitaura, K.; Katsumura, S. Abnormally High Reactivity of the Vinyl Hydrogen Toward Singlet Oxygen in Twisted 1,3-diene. *Tetrahedron Lett.* **1996**, *37*, 7771–7774.

- 23. Mori, H.; Ikoma, K.; Katsumura, S. Further Demonstration of the Higher Reactivity of the Vinyl Hydrogen Rather than the Allyl Hydrogen Towards Singlet Oxygen. *Chem. Comm.* 1997, 22, 2243–2244.
- 24. Mori, H., Ikoma, K., Isoe, S., Kitaura, K., & Katsumura, S. Photosensitized Oxygenation of Twisted 1,3-Dienes: Abnormally Higher Reactivity of Vinyl Hydrogen Rather than Allyl Hydrogen toward Singlet Oxygen. *J. Org. Chem.* 1998, 63, 8704–8718.
- 25. Delbaere, S.; Micheau, J.; Vermeersch, G. Multinuclear NMR Structural Characterization of an Unprecedented Photochromic Allene Intermediate. *Org. Lett.* **2002**, *4*, 3143–3145.
- 26. Olpp, T.; Brückner, R. Total Synthesis of the Light-Harvesting Carotenoid Peridinin. *Angew. Chem. Int. Ed.* **2006**, *45*, 4023–4027.
- 27. Macernis, M.; Streckaite, S.; Litvin, R.; Pascal, A. A.; Llansola-Portoles, M. J.; Robert, B.; Valkunas, L. Electronic and Vibrational Properties of Allene Carotenoids. *J. Phys. Chem. A* 2022, 126, 813–824.
- 28. Li, D. H.; Smith, B. D. Deuterated Indocyanine Green (ICG) with Extended Aqueous Storage Shelf-Life: Chemical and Clinical Implications. *Chem. Eur. J.* **2021**, *27*, 14535–14542.
- 29. Sugimoto, H.; Nakamura, S.; Ohwada, T. Retro-Diels-Alder Reaction of 4*H*-1,2-Benzoxazines to Generate *o*-Quinone Methides: Involvement of Highly Polarized Transition States. *J. Org. Chem.* **2007**, *72*, 10088–10095.
- 30. Khan, T. S.; Gupta, S.; Alam, M. I.; Haider, M. A. Reactivity Descriptor for Retro Diels-Alder Reaction of Partially Saturated 2-Pyrones: DFT Study on Substituents and Solvents Effect. *RSC Adv.* **2016**, *6*, 101697–101706.
- 31. Gupta, S.; Alam, M. I.; Khan, T. S.; Sinha, N.; Haider, M. A. On the Mechanism of Retro-Diels-Alder Reaction of Partially Saturated 2-Pyrones to Produce Biorenewable Chemicals. *RSC Adv.* **2016**, *6*, 60433–60445.
- 32. Ansari, E.S.; Ghiasi, R.; Forghaniha, A. Thermodynamic and Kinetic Studies of the Retro-Diels-Alder Reaction of 1,4-Cyclohexadiene, 4*H*-Pyran-4*H*-thiopyran, 1,4-Dioxine, and 1,4-Dithiine: A Theoretical Investigation. *Struct. Chem.* **2019**, *30*, 877–885.

- 33. Gorka, A. P.; Schnermann, M. J. Harnessing Cyanine Photooxidation: from Slowing Photobleaching to Near-IR Uuncaging. *Curr. Opin. Chem. Biol.* **2016**, *33*, 117-125.
- 34. Frisch, M. J.; Trucks, G. W.; Schlegel, H. B.; Scuseria, G. E.; Robb, M. A.; Cheeseman, J. R.; Scalmani, G.; Barone, V.; Mennucci, B.; Petersson, G. A. et al. Gaussian 16, Revision C.01; Gaussian, Inc.: Wallingford, CT, 2019.
- 35. Zhao, Y.; Truhlar, D. G. The M06 Suite of Density Functionals for Main Group Thermochemistry, Thermochemical Kinetics, Noncovalent Interactions, Excited States, and Transition Elements: Two New Functionals and Systematic Testing of Four M06-class Functionals and 12 other Functionals. *Theor. Chem. Acc.* **2008**, *120*, 215–241.
- 36. Hehre, W. J.; Ditchfield, R.; Pople, J. A. Self-Consistent Molecular Orbital Methods. XII. Further Extensions of Gaussian-Type Basis Sets for Use in Molecular Orbital Studies of Organic Molecules. *J. Chem. Phys.* **1972**, *56*, 2257–2261.
- 37. Hariharan, P. C.; Pople, J. A. The Influence of Polarization Functions on Molecular Orbital Hydrogenation Energies *Theor. Chim. Acta* **1973**, *28*, 213–222.
- 38. Clark, T.; Chandrasekhar, J.; Spitznagel, G. W.; Schleyer, P. V. R. Efficient Diffuse Function-Augmented Basis Sets for Anion Calculations. III. The 3-21+G Basis Set for First-row Elements, Li-F. *J. Comput. Chem.* **1983**, *4*, 294–301.
- 39. Ansari, E. S.; Ghiasi, R.; Forghaniha, A. Computational Investigation into the Solvent Effect on the Diels-Alder Reaction of Isobenzofuran and Ethylene. *Chem. Meth.* **2020**, *4*, 220–233.
- 40. Ahraminejad, M.; Ghiasi, R.; Mohtat, B.; Ahmadi, R. Substituent Effect in the [2 + 4] Diels-Alder Cycloaddition Reactions of Anthracene with C<sub>2</sub>X<sub>2</sub> (X = H, F, Cl, Me): A Computational Investigation. *J. Struct. Chem.* **2021**, 62, 1551–1562.
- 41. Jensen, F. Introduction to Computational Chemistry, 2<sup>nd</sup> ed.; Wiley: Chichester, U.K., 2007.
- Glendening, E. D.; Badenhoop, J. K.; Reed, A. E.; Carpenter, J. E.; Bohmann, J. A.; Morales,
   C. M.; Karafiloglou, P.; Landis, C. R.; Weinhold, F. NBO 7.0. Theoretical Chemistry
   Institute, University of Wisconsin, Madison, 2018.

- 43. Riplinger, C.; Sandhoefer, B.; Hansen, A.; Neese, F. Natural Triple Excitations in Local Coupled Cluster Calculations with Pair Natural Orbitals. *J. Chem. Phys.* **2013**, *139*, 134101–134113.
- 44. Guo, Y.; Riplinger, C.; Becker, U.; Liakos, D. G.; Minenkov, Y.; Cavallo, L.; Neese, F. Communication: An Improved Linear Scaling Perturbative Triples Correction for the Domain Based Local Pair-Natural Orbital Based Singles and Doubles Coupled Cluster Method [DLPNO-CCSD(T)]. *J. Chem. Phys.* 2018, 148, 11101–11105.
- 45. Dunning, T. H. Gaussian Basis Sets for Use in Correlated Molecular Calculations. I. The Atoms Boron Through Neon and Hydrogen. *J. Chem. Phys.* **1989**, *90*, 1007–1023.
- 46. Kendall, R. A.; Dunning, T. H.; Harrison, R. J. Electron Affinities of the First-row Atoms Revisited. Systematic Basis Sets and Wave Functions. *J. Chem. Phys.* **1992**, *96*, 6796–6806.